Density estimation based on *k*-tree sampling and point pattern reconstruction

Arne Nothdurft, Joachim Saborowski, Robert S. Nuske, and Dietrich Stoyan

Abstract: In *k*-tree sampling, also referred to as point-to-tree distance sampling, the *k* nearest trees are measured. The problem associated with *k*-tree sampling is its lack of unbiased density estimators. The presented density estimator based on point pattern reconstruction remedies that shortcoming. It requires the coordinates of all *k* trees. These coordinates are translated into a simulation window where they remain unchanged. Empirical cumulative distribution functions of intertree and location-to-tree distances estimated from the sample plots are set as target characteristics. Using the idea of simulated annealing, an optimal new tree pattern is constructed in the simulation window outside the *k*-tree samples. The reconstruction of the point pattern minimizes the contrast between the empirical cumulative distribution functions and their analogs for the simulated pattern. The density estimator is simply the tree density of the optimum pattern in the simulation window. The performance of the reconstruction-based density estimator is assessed for $k = 6$ and $k = 4$ based on systematic sampling grids regarding its potential application in forest inventories. Simulations are carried out using real stem maps (covering different stand densities and different types of spatial point patterns, such as regular, clustered, and random) as well as completely random patterns. The new density estimator proves to be empirically superior in terms of bias and root mean squared error compared with commonly used estimators. The reconstruction-based density estimator has biases smaller than 2%.

Résumé : En échantillonnage de *k* arbres, aussi appelé échantillonnage de *k* arbres selon leur distance, on mesure les *k* arbres les plus proches. Le problème lié à l'échantillonnage de *k* arbres est son incapacité à fournir des estimateurs de densité sans biais. L'estimateur de densité basé sur la reconstruction du patron des points comble cette lacune. Il requiert les coordonnées de tous les *k* arbres. Ces coordonnées sont traduites dans une fenêtre de simulation où elles demeurent inchangées. Les fonctions empiriques de distribution cumulative de distances entre les arbres et entre un point et les arbres estimées à partir des placettes échantillons sont les caractéristiques cibles. En utilisant le recuit simulé, un nouveau patron optimal des arbres est construit dans la fenêtre de simulation en dehors des *k* arbres échantillons. La reconstruction du patron de points minimise le contraste entre les fonctions empiriques et leurs analogues dérivés du patron simulé. L'estimateur de densité est tout simplement la densité des arbres de la structure optimale dans la fenêtre de simulation. La performance de l'estimateur de densité basé sur la reconstruction est évaluée pour $k = 6$ et $k = 4$ sur la base des grilles d'échantillonnage systématique quant à son application potentielle dans les inventaires forestiers. Des simulations sont effectuées en utilisant les cartes réelles des tiges (couvrant différentes densités de peuplement et différents types de patrons spatiaux de points, tels que régulier, en grappe et aléatoire) aussi bien que des patrons complètement aléatoires. Le nouvel estimateur de densité s'avère empiriquement supérieur en termes de biais et d'erreur quadratique moyenne par rapport aux estimateurs fréquemment utilisés. Son biais est inférieur à 2%.

[Traduit par la Rédaction]

Introduction

In *k*-tree sampling, also known as point-to-tree distance sampling, sample points are distributed as random or systematic samples in the surveyed forest. For each sample point, exactly *k* trees, the *k* nearest, are measured. *k*-tree sampling may yield unbiased estimators of forest structural variables such as tree species mingling indices or tree size differentiation. However, the statistical properties of *k*-tree sampling are known to be poor if applied for tree density estimation. This is because *k*-tree sampling leads to variable sample plot areas, since the plot radius is determined by the horizontal (slope adjusted) distance to the *k*th tree (Prodan 1968), with unknown inclusion probabilities for the sampled trees. This is in contrast with so-called fixed-radius sample plots with constant radius. *k*-tree sampling has never been

Received 25 May 2009. Accepted 14 February 2010. Published on the NRC Research Press Web site at cjfr.nrc.ca on 30 April 2010.

A. Nothdurft.[1] Forest Research Institute Baden-Württemberg, Department of Biometrics and Informatics, Post Box 79007, Freiburg 79100, Germany.
J. Saborowski. Department of Ecoinformatics, Biometrics and Forest Growth and Department of Ecosystem Modelling, University of Göttingen, Büsgenweg 4, Göttingen D 37077, Germany.
R.S. Nuske. Department of Ecoinformatics, Biometrics and Forest Growth, University of Göttingen, Büsgenweg 4, Göttingen D 37077, Germany.
D. Stoyan. TU Bergakademie Freiberg, Institute for Stochastics, Freiberg 09596, Germany.

[1]Corresponding author (e-mail: arne.nothdurft@online.de).

applied in national forest inventories, which is mainly because design-based statistical inference, the condicio sine qua non for acceptance by governmental agencies, lacks an unbiased density estimator.

k-tree sampling is nevertheless attractive, since the number of trees measured per plot is constant and the inventory costs are, therefore, nearly independent of tree density and easier to assess in advance. In the studies of Hall (1991), Lessard et al. (1994), and Lynch and Rusydi (1999), point-to-tree distance sampling proved to be more time and labor efficient than fixed-radius sampling. On average and over the past years, the forest service of the German federal state of Baden-Württemberg has paid to external contractors 12 euros per six-tree sample plot and 32 euros per sample plot with three fixed concentric radii. All trees with a diameter at breast height (DBH) ≥ 10 cm are measured in the innermost circle having a radius of 3 m whereas in the outer rings (r = 6 m and r = 12 m), trees with DBH ≥ 15 cm and DBH ≥ 30 cm, respectively, are surveyed. The considerable difference in unit costs is mainly due to reduced labor costs for *k*-tree sample plots because *k*-tree sample plots are usually performed single-handed whereas fixed-radius plots are surveyed by two workers. However, similar to fixed-radius plots, where additional measurements are often required for boundary trees, also on *k*-tree sample plots and especially in dense forest stands, one has to ensure to catch the true *k*th tree by control measurement. Besides its application in forest inventories, point-to-object distance sampling is also applied in ecological studies (Krebs 1998).

Because of its cost-saving nature, *k*-tree sampling is still applied in some places and many efforts have been undertaken to improve its statistical properties. In particular, in Baden-Württemberg, *k*-tree sampling is still applied and was often used in the past in combination with Prodan's (1968) classical density estimator $(k - 0.5)/F$ (in number of trees per hectare), with $F = \pi r_k^2/10\,000$ and r_k the distance to the *k*th tree in metres. Unfortunately, Prodan's density estimator is biased, which arises from incorrect tree inclusion probabilities. Therefore, and because of the economic attractiveness of *k*-tree sampling, attempts have been made to reduce this bias. See Magnussen et al. (2008) for an overview. Unbiased density estimators for *k*-tree sampling exist only for completely random point patterns (Sloboda 1976; Jonsson et al. 1992). Recently, a generally unbiased estimator was presented by Kleinn and Vilčko (2006*a*), which is based on inclusion zones by means of higher (*k*th)-order tessellations. To construct these tessellations, a large number of additional tree position have to be measured for each sample plot. This approach is no longer based on the original idea of *k*-tree sampling and is difficult to apply in the field (Kleinn and Vilčko 2006*a*) as well as costly when traditional measurement techniques are used. Kleinn and Vilčko (2006*b*) also presented an empirical method in which the sample plot radius is heuristically defined by the average of the distances to the *k*th and $(k + 1)$th tree. According to Magnussen et al. (2008), this is superior to other approaches, particularly for a small number of sample plots. Magnussen et al. (2008) provided two other parametric approaches for density estimation. The first approach, named ORBIT, constructs the sample plot area by summing up the areas of annuli of all *k* trees centered at the sample point. The inner radius r_0 of the nearest tree's annulus is chosen as $r_0 = \sqrt{\log 2} \times r_1$, with r_1 as distance of the nearest tree from the sample point, while the outer radius of the *k*th tree's annulus is predicted by linear regression. This estimator proved to be approximately unbiased for the completely random case in the study of Magnussen et al. (2008). The second estimator, named GAMPOI, is based on the assumption that the surveyed pattern arose from a so-called gamma-mixed Poisson process (Magnussen et al. 2008) and uses regression estimators for the parameters of the gamma distribution. Finally, Staupendahl (2008) presented a density estimator principally based on the work of Jonsson et al. (1992) but with an empirical bias correction that uses angle count indices.

This paper presents a completely different approach. The spatial structure of the sampled forest stand is reconstructed in a rectangular simulation window using the available *k*-tree sampling data and additional, simulated tree positions in the space between the sample plots. Finally, the density of the reconstructed pattern in the simulation window is used as an estimator of the true tree density. Apart from stationarity and isotropy, no additional model assumptions are used. This is an advantage over other more restrictive model-based approaches, which may easily fail if the actual pattern deviates considerably from the assumed model.

For the reconstruction, an iterative simulation technique is applied, which is based on the idea of simulated annealing (SA) (Kirkpatrick et al. 1983), an algorithm for optimization purposes. At first, the measured *k*-tree sample plots are transfered to the simulation window and additional trees are placed randomly within the simulation window but outside the sample plots. The point pattern is then iteratively changed by alternating between random generations of new tree locations and random deletions of existing trees. The criterion of optimality is a minimum contrast of summary characteristics for tree distances of both, the tree pattern on the original sample plots and the simulated tree pattern. The new density estimator for *k*-tree samples is called the reconstruction-based density estimator (RDE).

The approach of the present paper is inspired by the methods in Pommerening and Stoyan (2008) but differs in two important points: (*i*) the number of trees in the reconstruction forest is variable rather than fixed and it is just the parameter of interest and (*ii*) instead of reconstructing the entire forest, only a small fraction composed of small squares centered at the sample locations is reconstructed.

The departure from the approach of Pommerening and Stoyan (2008) in point *ii* facilitates efficient density estimation with respect to computing time. Our method is applicable if tree density estimation is of primary interest. In contrast, the method of Pommerening and Stoyan (2008) provides accurate reproductions with respect to tree species mingling and spatial differentiation of tree sizes.

The presented tree density estimator for *k*-tree sampling, which is based on nonparametric point pattern reconstructions, is applied for $k = 6$ and $k = 4$ to real stem maps of various densities and types of point patterns and to completely randomly generated tree patterns. The performance of the RDE is compared in terms of bias and root mean squared error (RMSE) with Prodan's (1968) classical density estimator and with the estimators of Kleinn and Vilčko (2006*b*), which

have shown to be the best performing estimators for small sample plot numbers in Magnussen et al. (2008).

Test data

The proposed RDE was applied to data of real forest stands as well as to simulated tree patterns. The real tree patterns were obtained from the data archive associated with the sampling simulator STIPSI (www.fva-bw.de/forschung/bui/stipsi_en.html) (Schöpfer 1967). A subset of six STIPSI stands was selected consisting of forest stands with the identification numbers 7, 21, 28, 30, 61, and 67 (Fig. 1; Table 1). The areas of the STIPSI stands range from 3.51 ha (STIPSI 28) to 7.76 ha (STIPSI 30). In addition, the RDE was applied to the publicly available longleaf pine (*Pinus palustris* P. Mill.) data (Platt et al. 1988; Cressie 1991). Following the criterion for merchantable wood in Germany, only trees with a DBH > 7 cm were analyzed in this study. Thus, 120 trees from the original 584 trees of the longleaf pine data were excluded. The selected forest stands meet three criteria: (1) contrasting stand conditions: monospecific (STIPSI 21 and longleaf pine) or almost monospecific (STIPSI 28), mixed species (STIPSI 7, STIPSI 30, STIPSI 61, and STIPSI 67), nearly even-aged (STIPSI 28), and uneven-aged (STIPSI 61), (2) a broad range of tree density: from 116 trees/ha (longleaf pine) to 878 trees/ha (STIPSI 67), and (3) divergent spatial tree patterns: regularity (STIPSI 21), clustering (STIPSI 7, STIPSI 30, and longleaf pine), and almost complete spatial randomness (STIPSI 28, STIPSI 61, and STIPSI 67).

With regard to criterion 3, the spatial tree patterns were characterized by pair correlation functions (Fig. 2). Regarding the estimation of the pair correlation functions shown in Fig. 2, we followed the recommendations of Illian et al. (2008). An aggregation is indicated, if the pair correlation function is above the horizontal reference line $g(r) \equiv 1$, whereas function values below suggest repulsion. The pair correlation functions in Fig. 2 indicate clustered tree patterns in the longleaf pine stand and in STIPSI 30 and STIPSI 7. The pair correlation function of STIPSI 21 seems to show some signs of regularity. STIPSI 21 and STIPSI 61 feature clearly softcore effects. The tree patterns of STIPSI 28, STIPSI 61, and STIPSI 67 are close to complete spatial randomness, especially at scales beyond the softcore effect.

The RDE was applied to the six STIPSI forest stands and the longleaf pine data based on 250 randomly placed grids of sample plot locations in each forest stand. While in practical forest inventory, only one sampling grid is applied, these 250 grids were used to determine sampling errors in a design-based approach.

Additionally, 1000 completely random patterns were simulated. Each pattern comprises 1000 trees in a 200 m × 200 m square window (250 trees/ha). These artificial tree populations serve as a database for a model-based evaluation of the RDE. This procedure reflects common practice of forest inventory where the estimation of tree density in a forest is based on one fixed sampling grid. The choice of 250 trees/ha as given tree density is of no relevance, since other tree densities can be obtained by a rescaling of the stem map. Thus, for a given location of a sample plot, always the same k trees are measured, independent of the current density.

Methods

Simulation of k-tree sampling

In accordance with Prodan (1968), $k = 6$ was chosen, which is a popular choice and a compromise between the two conflicting aims of considering a large number of trees and restricting measurement efforts.

The reconstruction-based density estimates of the STIPSI stands are obtained from n k-tree sample plots. In conformance with Prodan (1968), who suggested sample sizes of 4–6 sample plots/ha in each forest stand, the k-tree sample plots are arranged in a 50 m × 50 m sampling grid (Fig. 3). Applying fixed sampling grids to the relatively small populations the number of sample plots n may vary among the 250 different grids. Nevertheless, the average sample size can be expected to be 4 sample plots/ha with the applied 50 m × 50 m sampling grid.

The authors are aware that the sampling intensity of 4 plots/ha is relatively high with respect to inventories at the enterprise level. This results from the small sizes of all examined forest stands. If k-tree sampling is applied together with the RDE at enterprise level, the common grid widths of 100 or 200 m should be used.

The sample plots are shown in Fig. 3 as circles with a radius equal to the distances from the sample points to the corresponding sixth trees. In reality, the sample plots are no longer circular if their centers are closer to the forest stand border than to the corresponding sixth tree (see upper left and upper right sample plot in Fig. 3). For each forest stand, 250 density estimates are derived from 250 resamplings based on random shifts of the sampling grid, simulating a systematic sample selection with a random starting point.

In the simulated 1000 completely random tree patterns in 200 m × 200 m square windows, centered fixed sampling grids are laid out with $n = 9$, 16, or 25 sample plot locations (Fig. 4). The sample grid width is $200/\sqrt{n}$ with n being the number of sample plots. The smallest distance to the border of the square is $0.5 \times 200/\sqrt{n}$.

Additionally to $k = 6$, $k = 4$ was examined in the tree pattern of STIPSI 21, having some signs of regularity, in the longleaf pine stand, which shows the strongest clustering, and in the completely randomly generated patterns with $n = 9$ sample plots.

Summary characteristics of point patterns

Our approach is based on the idea of a realistic reconstruction of the spatial pattern of the trees outside the sample plot boundaries. A generated pattern is assumed to be an appropriate reconstruction if the distances between the simulated tree locations show the same distributional behavior as in the original forest stand. According to Tscheschel and Stoyan (2006), empirical cumulative distribution functions (ECDFs) of the distances to trees are used, namely the spherical contact distribution function and the nearest-neighbor distance distribution function are considered essential characteristics of spatial point patterns.

The true but unknown point process that generated the spatial arrangement of trees in an arbitrary forest stand is denoted by N; N is assumed to be stationary and isotropic. This is of course a strong and restrictive assumption, which

Fig. 1. Maps of tree positions and stand boundaries showing trees with DBH ≥ 7 cm; 7, 21, 28, 30, 61, and 67 are STIPSI stands (Schöpfer 1967) and LP is the longleaf pine data set (Platt et al. 1988).

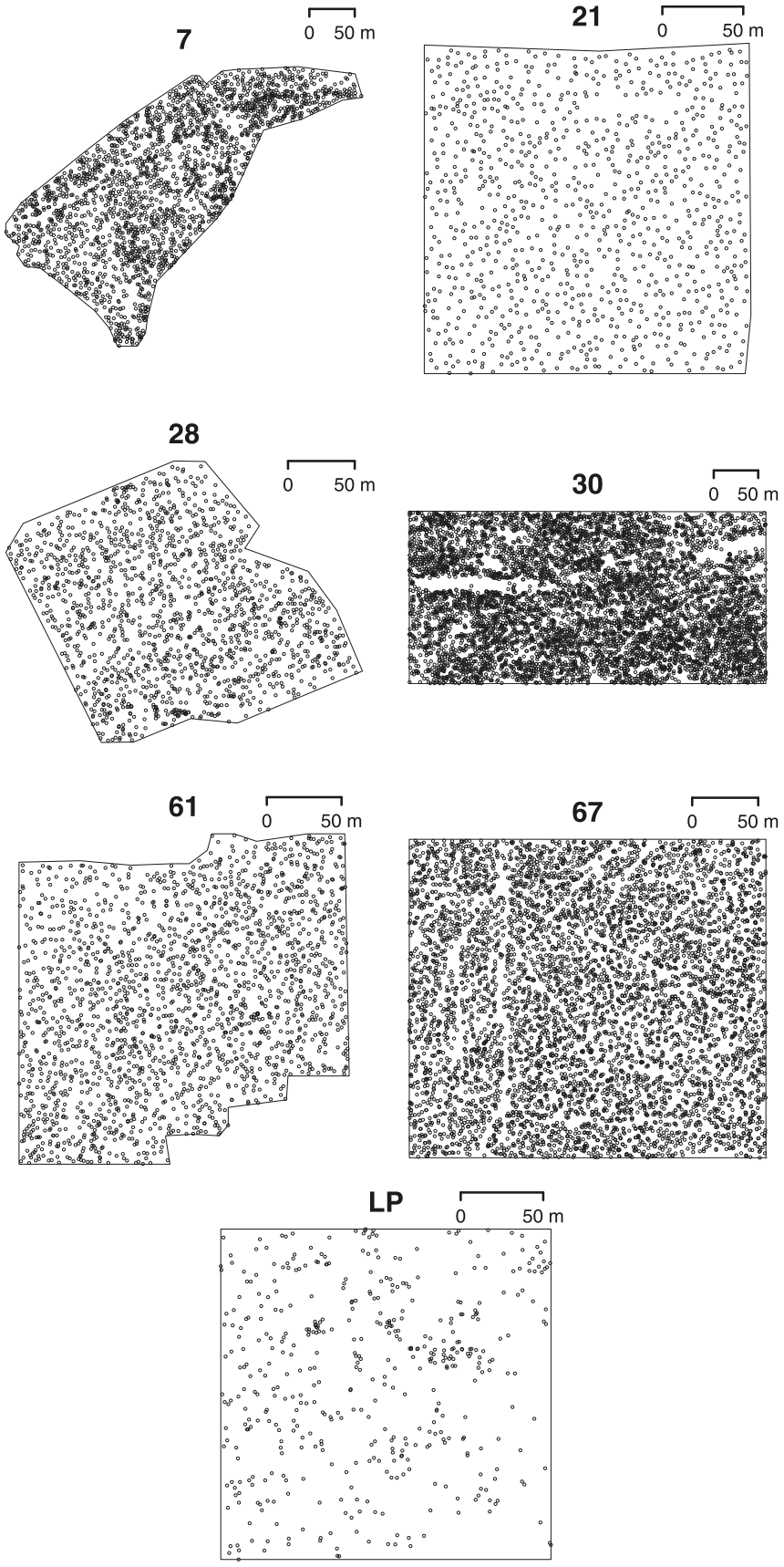

Table 1. Summary information on the analyzed forest stands.

ID	Species (%)	Age (range) (years)	Area (ha)	Trees/ha
7	Fir 60, beech 25, spruce 15	115 (110–120)	4.96	432
21	Beech 100	123 (110–140)	4.05	242
28	Spruce 95, others 5	127 (120–130)	3.51	421
30	Fir 40, spruce 40, pine 10, others 10	57 (50–60)	7.76	838
61	Beech 55, oak 30, hornbeam 10, fir 5	110 (90–120)	4.12	483
67	Oak 50, hornbeam 45, others 5	70 (60–75)	6.51	878
LP	Longleaf pine 100		4	116

Note: 7–67 are STIPSI stands (Schöpfer 1967) and LP is the longleaf pine data set (Platt et al. 1988). No information was available on the age of the trees of the longleaf pine data. From the original 584 trees, only the trees with DBH ≥ 7 cm were included.

is, however, often made in point process applications in forestry. $P(N(B) = 0)$ denotes the probability that there are no points (trees) in a specific subset B. If $B = b(o,r)$ is the disk of radius r centered at the origin o, the location-to-nearest-point distance distribution function is obtained, which is often called the spherical contact distribution function (Illian et al. 2008) or empty-space function (Baddeley and Gill 1997) and is formally defined as

$$[1] \qquad H_s(r) = 1 - P(N(b(o,r)) = 0) \text{ for } r \geq 0$$

Under the assumption that edge effects are of no importance, $H_s(r)$ can be estimated without bias from k-tree samples by considering only the distance of each sample point to its nearest trees. In this case and because of the stationarity, $P(N(b(o,r)) = 0)$ is simply estimated by the relative frequency of sample plots having no trees in a circle of radius r around the sample point.

Since the number n of sample plots was small, and therewith the number of origins to obtain $H_s(r)$, further distance measurements were necessary. Therefore, 10 measurement locations arranged in a regular grid were established in every sample plot (Fig. 5). From each of these 10 locations, in each of all n sample plots, the distance to the nearest tree on the sample plot was measured, and in total, $10n$ measurements were obtained. For these distances, the ECDF was calculated. The authors are aware of the fact that this strategy does not yield unbiased estimates of $H_s(r)$. The resulting ECDF, which is denoted by $\widehat{H}_s^k(r)$, may have some similarity to $H_s(r)$ but in fact estimates a different theoretical function $H_s^k(r)$; the upper index k refers to the context of k-tree sampling. The theoretical summary characteristic $H_s^k(r)$ can be rigorously defined for any stationary point process and is based on the distances from the 10 test points, as arranged in Fig. 5 around the origin o of the coordinate system (shown as a plus sign), to their nearest neighbors in $b(o,r_k)$, where r_k is the distance from o to the kth nearest tree. The sample point (plot center) was not used as a measurement location.

Tscheschel and Stoyan (2006) showed that point pattern reconstructions, such as described in the next section, work well if the location-related summary characteristic $H_s(r)$ is combined with a point-related summary characteristic. The natural choice for the latter is the nearest-neighbor distance distribution function:

$$[2] \qquad D(r) = P(N(b(o,r) \setminus \{o\}) > 0) \text{ for } r \geq 0$$

It gives the probability of finding the nearest neighbor of a tree within a disk of radius r centered at a tree location. The nearest-neighbor distance distribution function was first denoted by Diggle (1979) as $G(r)$. In this paper, the notation is that of Illian et al. (2008).

Due to the unequal probability selection of trees in k-tree sampling, an unbiased estimation of $D(r)$ based on k-tree samples is not possible. Just as in the case of $H_s(r)$, a new summary characteristic $D^k(r)$ is introduced, which is adapted to k-tree sample plots. This $D^k(r)$ is defined as the nearest-neighbor distance distribution function for the k trees of a k-tree sample plot. $D^k(r)$ is estimated by the ECDF corresponding to the nearest-neighbor distances of all $k \times n$ trees.

Finally, to improve the quality of reconstruction, not only the distances to the nearest neighbors are considered but also tree-to-tree distance ECDFs $D_l^k(r)$ corresponding to the distances from a tree to its lth neighbor with $l = 1, ..., k - 1$. Similarly, the location-to-tree distance ECDFs $H_{s,m}^k(r)$ of the distances to the mth neighbor with $m = 1, ..., k$ are considered. Thus, distances are measured from each tree to its $k - 1$ neighbors and likewise from each of the 10 test point locations to all of the k trees. This procedure yields $k(k - 1)n$ tree-to-tree distances and $k \times 10 \times n$ location-to-tree distances from all plots of the surveyed forest stand.

Reconstruction of spatial tree patterns

The algorithm to generate reconstruction-based density estimates is in the following described sequentially in a step-by-step manner.

Step 1: Estimate summary characteristics from original sample plots

A sample of n k-tree plots is selected from the forest stand of interest. The summary characteristics $D_l^k(r)$ and $H_{s,m}^k(r)$ are estimated on the original sample plots.

Step 2: Establish the simulation window

A rectangular simulation window W is constructed as a union of identical small squares arranged in the plane (see Figs. 4 and 6). The square side length is twice the size of the largest radius from the n k-tree sample plots. The centers of the squares correspond to the original sample points. It may happen that some squares in W do not contain a sample plot, such as the two in the upper right corner of Fig. 6. The sample points can be arranged arbitrarily in W. To minimize edge effects, the difference of the edge lengths of W in the x and y directions should be kept as small as possible. If $\sqrt{n}$ is an integer, the number of squares in W is equal in both

Fig. 2. Pair correlation functions of all trees having a DBH ≥ 7 cm; 7, 21, 28, 30, 61, and 67 are STIPSI stands and LP is the longleaf pine data set. Black line, estimated function; white line, theoretical value of the function under the null hypothesis of complete spatial randomness; gray area, 95% confidence envelope under the null hypothesis computed by Monte Carlo simulation using the fifth highest/lowest value of 199 replicates. Values $g(r) < 1$ suggest inhibition between points and values $g(r) > 1$ suggest clustering.

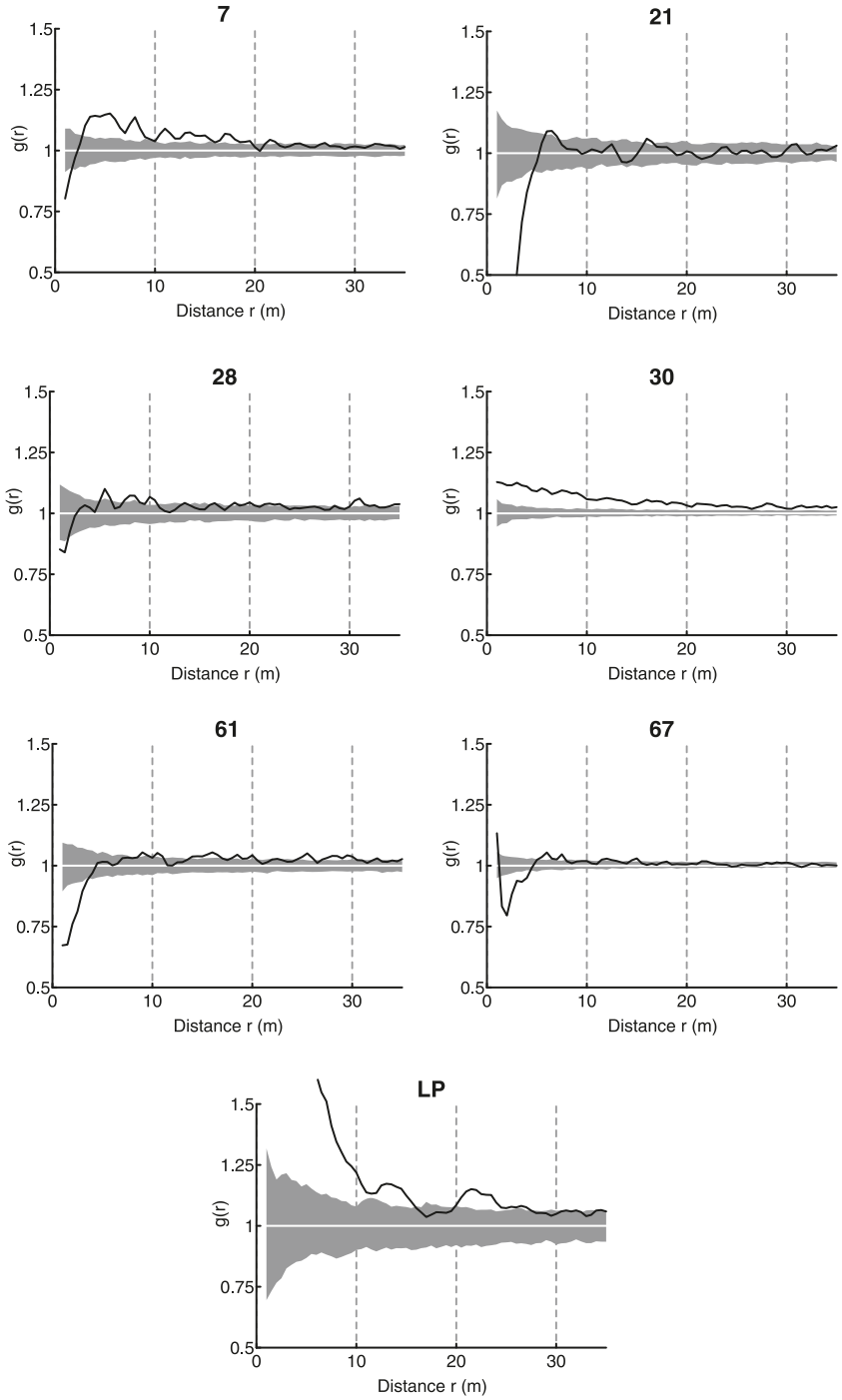

the x and y directions; for other cases, the number of squares in the x direction is set to trunc$[\sqrt{n}] + 1$.

Step 3: Translate the tree locations into the simulation window

The measured trees are translated from the original sample plots into the artificial simulation window W. Their original locations are kept fixed relative to the sample points. The sample plot area within each square is defined by the original shape, meaning that the sample plot areas that are reduced by intersection with the area of the forest stand are taken as cut disks; see the last sample plot in the first and second row in the simulation window of Fig. 6.

Step 4: Generate a point pattern as start configuration

The start configuration of the point pattern in the entire

Fig. 3. Positions of trees in a forest stand (STIPSI 28). Fourteen six-tree sample plots (large circles) are placed in a regular 50 m grid with a random start. Measured trees are shown as solid circles.

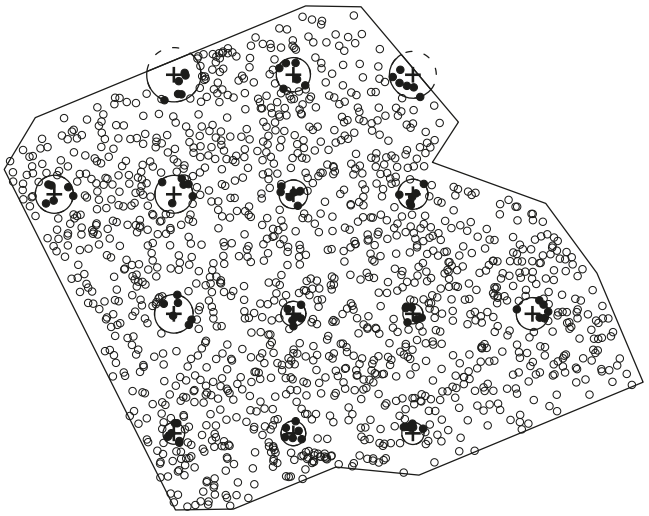

simulation window W is formed by the $k \times n$ measured trees plus newly generated points, which are scattered completely randomly in W outside the n fixed k-tree sample plots. The total number of points in W is chosen by means of Prodan's (biased) density estimator multiplied by the simulation window area. One could also choose different initial tree numbers, but the estimate used here provides a sufficiently realistic starting point leading to shorter computation times.

Step 5: Construct a virtual sampling grid

A dense triangle grid of p virtual k-tree sample plots is constructed in W to estimate the $D_l^k(r)$ and $H_{s,m}^k(r)$ for the simulated pattern in W. The resulting sample plots are shown as broken circles in Fig. 7 and the corresponding sample points are marked as crosses. The minimum distance between any two of p virtual sample points is twice the minimal radius of the original k-tree sample plots. The grid is placed centrally in W with equal distances from the outmost sample points to the nearest border of W. This guarantees a dense but also homogeneous and efficient coverage of the simulation window. On each virtual sample plot, the inter-tree distances and location-to-tree distances are measured and the same summary characteristics are obtained as for the actual tree locations on the original sample plots.

Step 6: Perform simulated annealing: accept/reject iterations

The next five substeps describe the SA algorithm. In an iterative manner, proposals of deletion and addition of trees in W are checked. The proposed change in the point pattern may result either in an improvement or in a degradation. The change is evaluated by a contrast measure C_t. It is based on the sum of squared differences between the ECDFs $D_l^k(r)$ and $H_{s,m}^k(r)$ corresponding to the original sample plots and the p virtual k-tree plots in the simulation window; see Step 6.4 for details. If a proposal causes improvement, the new state of the point pattern is accepted and otherwise rejected. In the latter case, the point pattern is reset to the prior state.

The core algorithm is a loop over Steps 6.1–6.5. The runs are denoted by t, the index of iteration. The iteration is carried out $10Q$ times where Q is the initial number of trees in the simulation window outside the transferred sample plots. The whole sequence of iterations is given by $t = 1, ..., 10Q$.

Step 6.1: Propose a deletion or an addition

In each $(2t - 1)$th iteration, one tree is deleted at random, and in each $(2t)$th iteration, one tree is generated at random.

The location of a possible new tree is generated by two uniformly distributed decimal random numbers for its x- and y-coordinates within W but outside the n fixed sample plots.

An existing tree from outside the fixed sample plots is deleted if its identification number corresponds to a generated integer random number, which is uniformly distributed over the range of all possible tree identification numbers. Since the number of trees in W outside the fixed sample plots varies, new tree identification numbers are continuously allocated after each iteration.

Whereas the addition of a tree follows complete randomness, the deletion is performed as simple random sampling from a list. According to the principle of conditional simulation (Illian et al. 2008), the translated and fixed k-tree sample plots in the simulation window are not affected by deletions and generations.

Step 6.2: Perform k*-tree sampling in the simulation window*

The point pattern is changed by a deletion and an addition. Therefore, a new k-tree sampling is performed in W based on the fixed triangle grid of sample points. For each of the p virtual sample points, the tree locations of the k nearest trees are recorded.

Step 6.3: Estimate summary characteristics from virtual sample plots

After each change of the simulated point pattern, caused by a deletion or an addition, it must be decided to which extent the summary characteristics of the new pattern in W deviate from $\widehat{D}_l^k(r)$ and $\widehat{H}_{s,m}^k(r)$, which were obtained from the n original k-tree plots. For this purpose, the summary characteristics $D_l^k(r)$ and $H_{s,m}^k(r)$ are newly estimated in the reconstruction window W. The $k - 1$ point-related nearest-neighbor distribution functions $D_l^k(r|t)$ for $l = 1, ..., k - 1$ and the k location-related spherical contact distribution functions $H_{s,m}^k(r|t)$ for $m = 1, ..., k$ are estimated by means of the grid of the p virtual sample plots, where $|t$ indicates the dependence on the current number t of iterations carried out.

Step 6.4: Measure the contrast

The decision about the acceptance of a deletion or addition is based on a contrast measure C_t (eq. 3 below), which is calculated after every iteration t. The first summand of eq. 3 is the sum of squared deviations between the ECDFs of the nearest-neighbor distances, where the distribution functions $\widehat{D}_l^k(i\delta)$ result from the n sample plots in the original forest stand and the distribution functions $\widehat{D}_l^k(i\delta|t)$ are derived after each iteration t from the simulation window by means of the virtual sample plots. The second summand in eq. 3 corresponds to the sum of squared distances between the ECDFs of the location-to-tree distances $\widehat{H}_{s,m}^k(j\delta)$

Fig. 4. Original six-tree samples with grids consisting of nine plots (top panels), 16 plots (middle panels), and 25 plots (bottom panels) in a simulated random point pattern with a density of 250 trees/ha (left panels) and the corresponding reconstructed tree patterns in the virtual simulation window W (right panels). W is constructed as a union of identical squares (broken lines) with side length of twice the largest radius from the six-tree sample plots. The panels on the right are rescaled to fill the entire figure region.

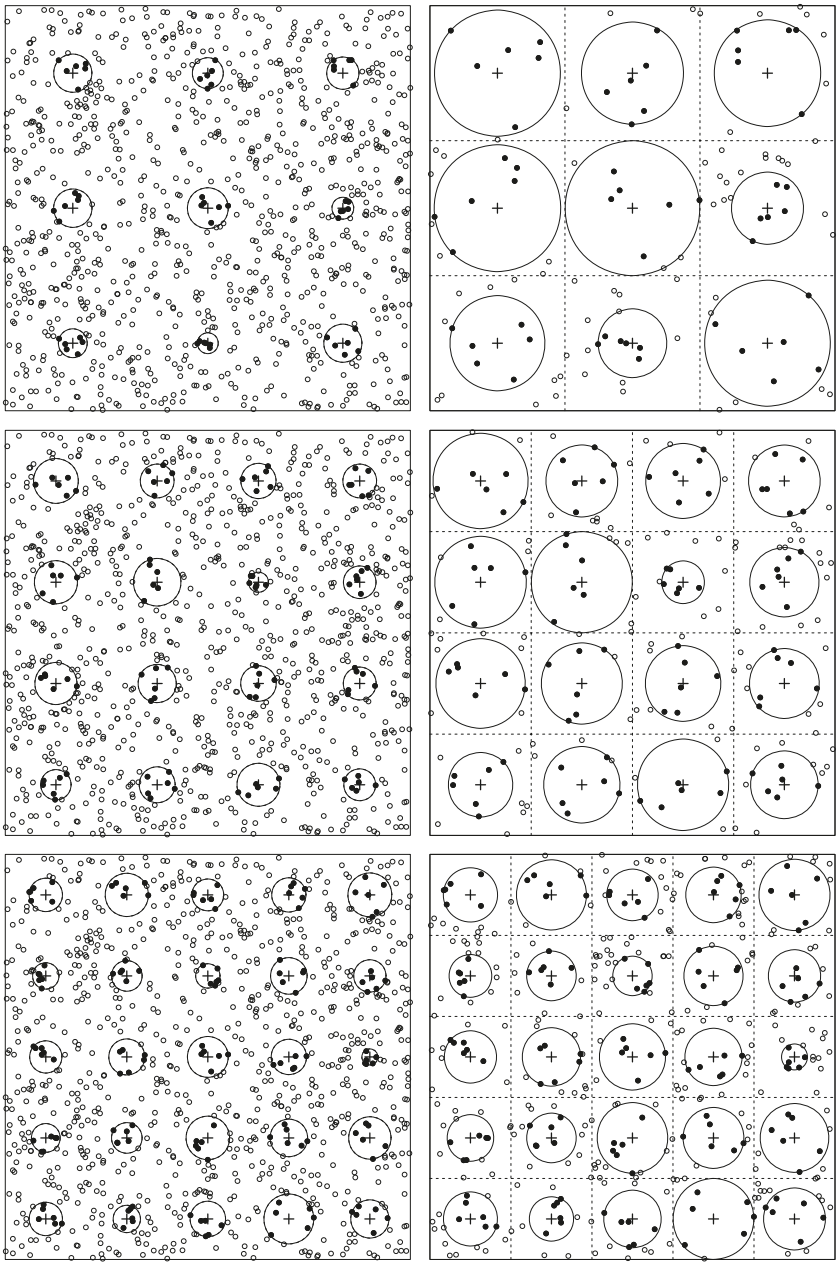

obtained from the n sample plots and $\widehat{H}^k_{s,m}(j\delta|t)$ from the p virtual sample plots in W. The ECDFs are based on distance classes of width $\delta = 0.2$ m. The total number of classes for $\widehat{D}^k_l$ is n_D and that for $\widehat{H}^k_{s,m}$ is n_H. Both depend on the sampling geometry.

The contrast function, i.e., the overall sum of squared differences between the estimates of the distribution functions, is

$$[3] \qquad C_t = \sum_{l=1}^{k-1}\sum_{i=1}^{n_D}\left(\widehat{D}^k_l(i\delta) - \widehat{D}^k_l(i\delta|t)\right)^2 + \sum_{m=1}^{k}\sum_{j=1}^{n_H}\left(\widehat{H}^k_{s,m}(j\delta) - \widehat{H}^k_{s,m}(j\delta|t)\right)^2$$

Fig. 5. The 10 regularly arranged test point locations (crosses) for measurement of location-to-tree distances in a six-tree sample plot. Measured trees are shown as solid circles and the sample point is depicted as a plus sign.

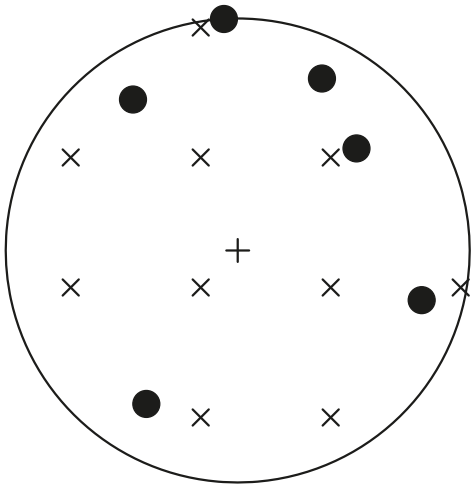

It seems natural to assume that for accurate point pattern reconstructions, all intertree distances and all location-to-tree distances are of the same relevance. Therefore, all terms in eq. 3 are of equal weight.

Step 6.5: Decide: accept or reject

If the contrast measure is reduced in an iteration t, i.e., if $C_t < C_{t-1}$, an improvement is obtained and the new state of the point pattern is accepted. Otherwise, the new state is rejected, and the point pattern in the simulation window is reset to the previous configuration.

After the decision is made, the algorithm switches again to Step 6.1, so long as the number of iterations is smaller than $10Q$. Otherwise, the next step is the final Step 7.

Step 7: Estimate the density from a subset of the simulation window

It is known from simulation studies for point pattern generation that a "drift towards the boundary" effect may occur, meaning point locations at the edge of the simulation window are preferred (Illian et al. 2008). To eliminate this effect's influence on density estimates, the density is estimated from a rectangular subwindow W^* within the simulation window (broken square in Fig. 7). The subwindow is constructed by subtracting an inner frame of width equal to the maximum radius of the original sample plots from simulation window. With the area of the subwindow $|W^*|$ and N^* the final number of trees in W^* the density estimator is

$$[4] \qquad \hat{\lambda} = \frac{N^*}{|W^*|}$$

Additional remarks

The accept/reject algorithm applied here corresponds to SA (Kirkpatrick et al. 1983). Although, the original SA algorithm allows the acceptance of statuses where $C_t > C_{t-1}$ with small probability, we use an improvements-only algorithm, as described in Tscheschel and Stoyan (2006). The SA algorithm is a global optimization method; the improvements-only algorithm may in some cases only find local optima. Tscheschel and Stoyan (2006) compared the classical SA algorithm with the faster improvements-only algorithm and found that the improvements-only algorithm is sufficient for good point pattern reconstruction.

During the iterations, deletions and additions (Step 6.1) are *proposed* in alteration. However, this does not mean that each deletion that *occurred* is followed by an addition. It is possible that a proposed addition is withdrawn after an accepted deletion because no improvement of the point pattern was achieved, so the next event is again a deletion. The opposite situation, the withdrawal of a proposed deletion after an accepted addition, may also occur.

Figure 8 shows the empirical distribution functions of the summary characteristics that were estimated from the k-tree sample plots in STIPSI 28 (solid curves) and those obtained from the dense triangle grid of virtual k-tree sample plots in the simulation window W (dotted curves) in Step 6.3. The curves for the ECDFs from the simulation window in the upper two graphs are obtained from the initial state ($t = 1$) of the SA algorithm; the dotted curves in the lower two graphs are obtained in the final iteration. The differences between the solid and dotted curves, and therefore the contrast, is remarkably reduced (see also Fig. 9). The ECDFs from the original sample plots and those from the virtual sample plots in W become almost identical.

Comparison of performances

According to the study of Magnussen et al. (2008), the best performing density estimator in terms of bias for k-tree sampling with $n \leq 20$ is the estimator of Kleinn and Vilčko (2006*b*). Originally, they proposed two density estimators in which the sample plot radius is calculated by an average of the distances to the kth tree (r_k) and the $(k + 1)$th tree (r_{k+1}). The first estimator uses the arithmetic mean of both distances $0.5(r_k + r_{k+1})$ and the second uses the quadratic mean $\sqrt{0.5(r_k^2 + r_{k+1}^2)}$. The corresponding estimates are henceforth referred to as KV1 and KV2. Since these estimators do not only depend on the distance to the kth tree, but also to the $(k + 1)$th tree, they are $(k + 1)$-tree sampling approaches. Therefore, the performances of KV1 and KV2 were examined for given k ($KV1_{k,k+1}$ and $KV2_{k,k+1}$) and for $k - 1$ ($KV1_{k-1,k}$ and $KV2_{k-1,k}$). In the following, for $k = 6$ and $k = 4$, the performance of the RDE is compared with $KV1_{k,k+1}$, $KV2_{k,k+1}$, $KV1_{k-1,k}$, $KV2_{k-1,k}$, and Prodan's estimator.

Results

Real stem maps for $k = 6$

The biases of the RDE for $k = 6$ range from 0 trees/ha in STIPSI 61 to +4.3 trees/ha (+1.8%) in STIPSI 21 (Table 2). According to the small observed biases, the RDE proved to be approximately unbiased for all STIPSI stands. In contrast, the estimator of Prodan (1968) is seriously biased. It overestimated the tree density from +12.6 trees/ha (+5.2%) in STIPSI 21 to +44.1 trees/ha (+10.5%) in STIPSI 28.

Both density estimators of Kleinn and Vilčko (2006*b*) also showed considerable biases in all STIPSI stands (Table 2) and were positively correlated with the biases of Prodan's estimator. The KV1 estimator of Kleinn and

Fig. 6. Artificial simulation window W resulting from Fig. 3 with fixed tree locations (small solid circles) within the $n = 14$ transferred six-tree sample plots (large circles) and simulated tree positions (small open circles). W is constructed as a union of identical squares (broken lines) with side length of twice the largest radius from the six-tree sample plots.

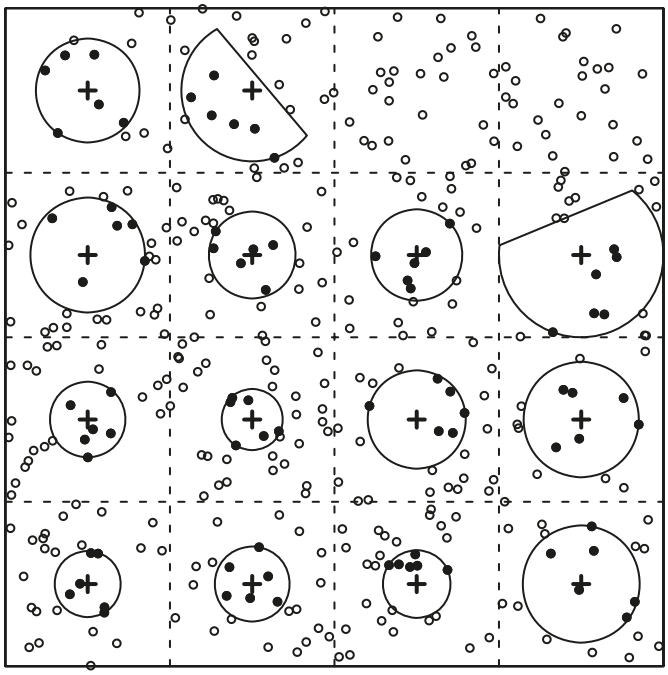

Fig. 7. Artificial simulation window W derived from Fig. 3 with fixed tree locations (small solid circles) within the $n = 14$ transferred six-tree sample plots (large circles) arranged in a regular grid (plus signs) and with the simulated tree positions (small open circles). The nearest-neighbor summary characteristics of the simulated tree patterns are obtained from measurements on $p = 68$ six-tree sample plots (large broken circles) arranged in a dense triangle grid (crosses). The final density estimate is obtained from the subwindow W^* (broken square).

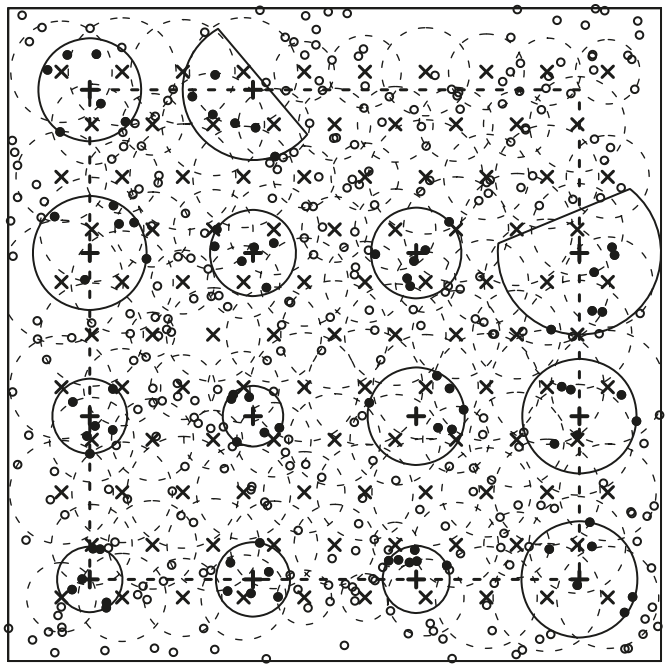

Vilčko (2006*b*) with $k = 6$ ($KV1_{6,7}$) overestimated the tree density from +10 trees/ha (+4.1%) in STIPSI 21 to +82.3 trees/ha (+9.8%) in STIPSI 30 and with $k = 5$ ($KV1_{5,6}$) from +12.8 trees/ha (+5.3%) to +108.3 trees/ha (+12.9%) in STIPSI 30. The biases of the KV2 estimator with $k = 6$ ($KV2_{6,7}$) range from +9.1 trees/ha (+3.8%) in STIPSI 21 to +78.7 trees/ha (+9.4%) in STIPSI 30 and with $k = 5$ ($KV2_{5,6}$) from +11.5 trees/ha (+4.8%) to +103 trees/ha (+12.3%).

Fig. 8. Empirical cumulative distribution functions (ECDF) of the nearest-neighbor summary characteristics. The solid curves were obtained from the 14 original six-tree sample plots in STIPSI 28 and the dotted curves from the 68 virtual six-tree sample plots arranged in a dense triangle grid in the simulation window. The panels on the left-hand side show the ECDFs of intertree distances. Starting from the left, the curves correspond to the l = 1, ..., 5th neighbor. The panels on the right-hand side show the ECDFs of location-to-tree distances. From the left to the right, the curves correspond to the m = 1, ..., 6th tree. The dotted curves in the upper panels were obtained from the initial pattern at the beginning of the SA iterations and those in the lower panels from the tree pattern in the final state of the SA algorithm. The sum of squared differences between the solid curves (original sample plots) and the dotted curves (simulation window) was used as a contrast measurement.

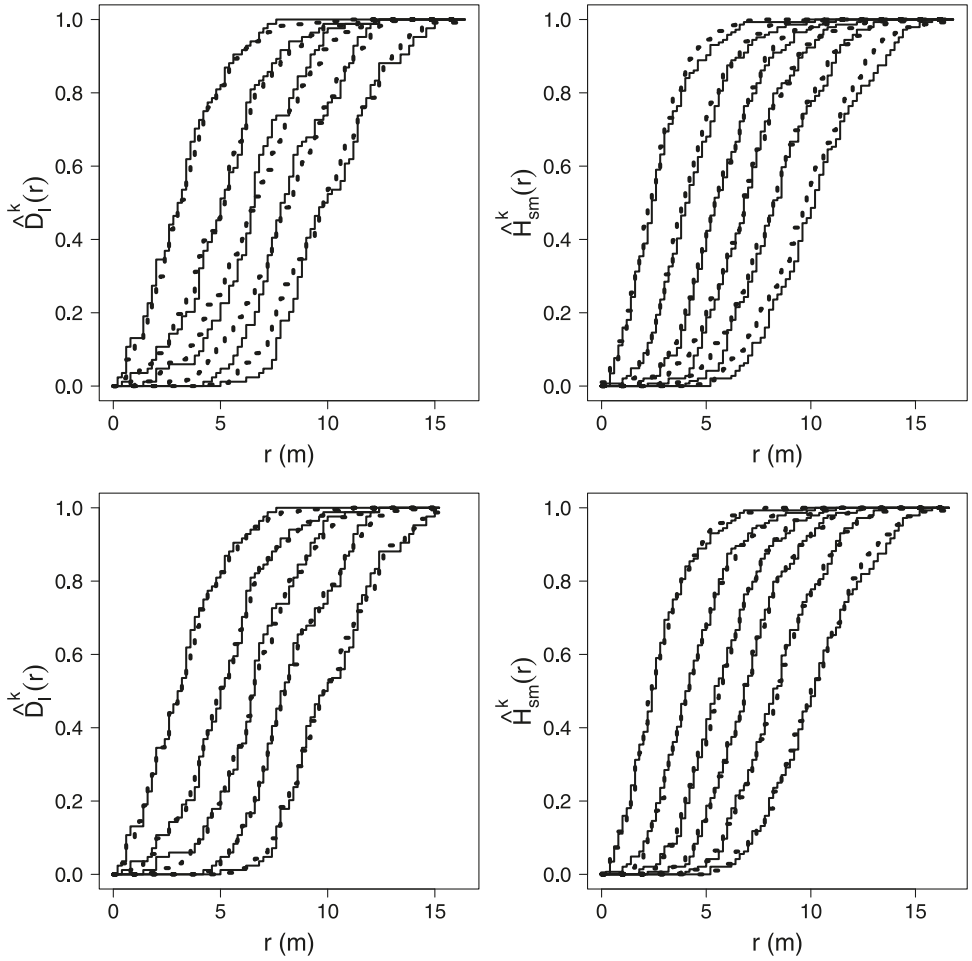

Fig. 9. Realizations of tree density during the SA algorithm. Density estimates (solid line, left axis) and contrast measure C_t (broken line, right axis) over the number of iterations. There were 2940 (=10Q) iterations (x-axis) carried out, since 294 (=Q) trees were initially placed in the simulation window between the fixed sample plots.

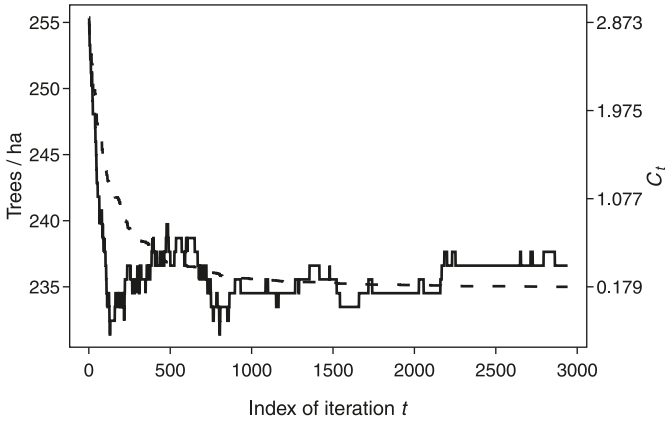

For the tree pattern of the reduced longleaf pine data set and with k = 6, the RDE achieved a bias of –0.2 tree/ha (–0.2%) whereas the other estimators showed much larger biases: $KV1_{6,7}$, 21.7 trees/ha (+18.7%); $KV2_{6,7}$, 21.1 trees/ha (+18.2%); $KV1_{5,6}$, 22.7 trees/ha (+19.5%); $KV2_{5,6}$, 21.9 trees/ha (+18.8%); Prodan, 17.1 trees/ha (+14.8%).

The RDE's density estimates of all analyzed real tree patterns have smaller RMSEs than those of Prodan's estimator and also smaller than the RMSEs of KV1 and KV2 (Table 2) for k = 5. Except for STIPSI 21, the RDE also achieved smaller RMSEs compared with KV1 and KV2 for k = 6.

The general trends show that the RDE reduced the bias by a factor of at least 3 compared with Prodan's estimator and by a factor of at least 2 compared with the KV estimators. The biases of the RDE were below 2% for all real stem maps. The largest bias of the RDE (1.8%) can be observed in the tree pattern of STIPSI 21, which shows some signs of regularity. And only for this tree pattern did the KV estimators with usage of the distance to the seventh tree show

Table 2. Simulation results with $k = 6$ (RDE, $KV1_{6,7}$, $KV2_{6,7}$, and Prodan) and $k = 5$ ($KV1_{5,6}$ and $KV2_{5,6}$).

		RDE			$KV1_{6,7}$			$KV2_{6,7}$			Prodan			$KV1_{5,6}$			$KV2_{5,6}$		
ID	Trees/ha	Mean	Bias (%)	RMSE	Mean	Bias (%)	RMSE	Mean	Bias (%)	RMSE	Mean	Bias (%)	RMSE	Mean	Bias (%)	RMSE	Mean	Bias (%)	RMSE
7	431.9	428.6	–0.7	43.1	469.6	8.7	57.8	467.9	8.3	56.4	471.6	9.2	64.5	474.4	9.8	66.9	472.0	9.3	65.1
21	241.9	246.2	1.8	18.2	251.9	4.1	17.7	251.0	3.8	17.2	254.5	5.2	20.9	254.7	5.3	20.1	253.4	4.8	19.2
28	420.7	427.2	1.5	45.7	456.9	8.6	62.8	455.2	8.2	61.5	464.8	10.5	69.4	463.5	10.2	69.5	461.0	9.6	67.6
30	837.7	830.6	–0.9	92.3	920.0	9.8	125.0	916.4	9.4	122.3	920.3	9.9	124.5	946.0	12.9	144.5	940.7	12.3	139.9
61	483.3	483.3	0.0	46.4	514.1	6.4	53.7	512.1	6.0	52.3	518.8	7.4	60.3	516.5	6.9	58.9	513.6	6.3	56.7
67	878.4	879.6	0.1	78.1	945.7	7.7	102.9	941.9	7.2	100.2	955.3	8.7	122.4	963.9	9.7	123.7	958.0	9.1	118.9
LP	116.0	115.8	–0.2	27.3	137.7	18.7	43.0	137.1	18.2	42.5	132.4	14.1	38.6	138.7	19.5	46.4	137.9	18.8	45.7

Note: 7–67 are STIPSI stands and LP is the longleaf pine data set.

slightly smaller RMSEs (RDE, 18.2; $KV1_{6,7}$, 17.7; $KV2_{6,7}$, 17.2).

In comparison with Prodan's estimator, the RMSEs were reduced by 13%–37%, and by at least 11%–41% compared with the different KV estimators, excluding the results in STIPSI 21. In summary, the RDE approach not only provides nearly unbiased estimates but also its RMSEs are mostly smaller than those obtained from the other estimators.

Random patterns for $k = 6$

The biases of the RDE in 1000 random point patterns were +1.7 trees/ha (+0.7%) for the nine-sample plots, +1.1 trees/ha (+0.4%) for the 16-sample plots, and +0.3 tree/ha (+0.1%) for the 25-sample plots (Table 3). Prodan's estimator, in contrast, showed serious biases for the random pattern of +23.0 trees/ha (+9.2%) for the nine-sample plots, +25.6 trees/ha (+10.3%) for the 16-sample plots, and +23.8 trees/ha (+9.5%) for the 25-sample plots.

Regarding the STIPSI stands, the KV1 and KV2 density estimators also proved to be biased, where the biases were positively correlated with those from Prodan's estimator. The KV1 estimator with $k = 6$ ($KV1_{6,7}$) showed a bias of +21.6 trees/ha (+8.6%) for the nine-sample plots, +22.7 trees/ha (+9.1%) for the 16-sample plots, and +21.7 trees/ha (+8.7%) for the 25-sample plots. The biases of the KV2 estimator with $k = 6$ ($KV2_{6,7}$) were slightly smaller: +20.5 trees/ha (+8.2%) for nine-sample plots, +21.6 trees/ha (+8.6%) for 16-sample plots, and +20.6 trees/ha (+8.3%) for 25-sample plots. The bias increased for all applied sample sizes when the KV estimators were applied with $k = 5$ instead of $k = 6$.

For the three sampling grids with nine-, 16-, and 25-sample plots, the RDE showed smaller RMSEs than the other estimators in this comparison (Table 3).

Compared with the other estimators, the bias was reduced by a factor of at least 12 by the RDE for random patterns. The biases of the RDE were below 1% for all three sample sizes. Applying the RDE to nine-sample plots, the RMSE was lowered by about 9% in comparison with Prodan's estimator and by at least 2% compared with the KV estimators. With 16-sample plots, the RMSE was reduced by 27% in comparison with Prodan's estimator and by at least 17% compared with the KV estimators. Using 25-sample plots, the RMSE of the RDE was 31% smaller than the RMSE of Prodan's estimator and at least 21% smaller than those obtained by the KV estimators.

The bias of all estimators did not vary remarkably for different sample sizes of nine, 16, and 25 plots, but the RMSEs were significantly reduced by larger sample sizes.

Subset of real stem maps and random patterns for $k = 4$

For $k = 4$ in the random tree patterns, the bias of the RDE was 2.9% and the biases of the KV estimators were 12.4% ($KV1_{4,5}$), 11.5% ($KV2_{4,5}$), 17.3% ($KV1_{3,4}$), and 15.3% ($KV2_{3,4}$) (see Table 4). Prodan's estimator showed a bias of 17.9% for $k = 4$ in the random patterns. In the random tree patterns, the RMSE of the RDE (59.2) was 5% smaller compared with $KV1_{4,5}$ (62.7), 2% smaller compared with $KV2_{4,5}$ (60.7), 31% smaller compared with $KV1_{3,4}$ (85.4), 27%

Table 3. Model-based simulation results with $k = 6$ (RDE, $KV1_{6,7}$, $KV2_{6,7}$, and Prodan) and $k = 5$ ($KV1_{5,6}$ and $KV2_{5,6}$) in 1000 point patterns generated by a binomial process with a density of 250 trees/ha.

	RDE			$KV1_{6,7}$			$KV2_{6,7}$			Prodan			$KV1_{5,6}$			$KV2_{5,6}$		
Sample plots	Mean	Bias (%)	RMSE	Mean	Bias (%)	RMSE	Mean	Bias (%)	RMSE	Mean	Bias (%)	RMSE	Mean	Bias (%)	RMSE	Mean	Bias (%)	RMSE
9	251.7	0.7	44.2	271.6	8.6	45.9	270.5	8.2	45.0	273.0	9.2	48.7	275.4	10.2	52.2	273.9	9.5	51.0
16	251.1	0.4	30.5	272.7	9.1	37.6	271.6	8.6	36.8	275.6	10.3	41.8	275.5	10.2	42.6	274.0	9.6	41.3
25	250.3	0.1	23.9	271.7	8.7	31.3	270.6	8.3	30.4	273.8	9.5	34.7	275.2	10.1	36.3	273.7	9.5	35.0

smaller compared with $KV2_{3,4}$ (81.0), and 28% smaller compared with Prodan's estimator (82.6).

In STIPSI 21, the RDE showed a bias of 3.1% and the biases of the KV estimators were 7.0% ($KV1_{4,5}$), 6.2% ($KV2_{4,5}$), 7.0% ($KV1_{3,4}$), and 5.6% ($KV2_{3,4}$). The bias of Prodan's estimator for $k = 4$ in STIPSI 21 was 8.5%. The RMSE of the RDE in STIPSI 21 (26.8) was 3% larger than the RMSE of $KV1_{4,5}$ (26.0), 9% larger than the RMSE of $KV2_{4,5}$ (24.6), 3% smaller than the RMSE of $KV1_{3,4}$ (27.7), 6% larger than the RMSE of $KV2_{3,4}$ (25.4), and 17% smaller than the RMSE of Prodan's estimator (32.3).

For $k = 4$ in the longleaf pine stand, the bias of the RDE was –0.2% and the KV estimators achieved biases of 23.2% ($KV1_{4,5}$), 22.2% ($KV2_{4,5}$), 26.0% ($KV1_{3,4}$), and 23.9% ($KV2_{3,4}$). Prodan's estimator showed a bias of 22.0% for $k = 4$ in the longleaf pine stand. The RMSE of the RDE (31.1) for the longleaf pine data was 43% smaller compared with $KV1_{4,5}$ (54.9), 42% smaller compared with $KV2_{4,5}$ (54.0), 44% smaller compared with $KV1_{3,4}$ (55.8), 42% smaller compared with $KV2_{3,4}$ (53.6), and 38% smaller compared with Prodan's estimator (50.1).

The application of $k = 4$ in the completely randomly generated tree patterns increased the bias of the RDE by a factor of 4.2 compared with $k = 6$. The choice of $k = 4$ instead of $k = 6$ increased the bias for the KV estimators by at least 40% ($KV2_{k,k+1}$) and by maximal 70% ($KV1_{k-1,k}$) in the random tree patterns. The bias of Prodan's estimator was 95% larger for $k = 4$ compared with $k = 6$. In STIPSI 21, the bias of the RDE was increased by 72% for $k = 4$ compared with $k = 6$ and the increase in bias for the KV estimators was between 17% ($KV2_{k-1,k}$) and 69% ($KV1_{k,k+1}$). The bias of Prodan's estimator was increased by 63% when using $k = 4$ instead of $k = 6$. In the longleaf pine data, the bias of the RDE was increased by 6% for $k = 4$ compared with $k = 6$. The bias increase of the KV estimators was between 22% ($KV2_{k,k+1}$) and 33% ($KV1_{k-1,k}$) and was 56% for Prodan's estimator.

For $k = 4$ compared with $k = 6$ in the completely randomly generated tree patterns, the RMSE of the RDE was increased by 34% and the KV estimators showed increases in RMSE between 35% ($KV2_{k,k+1}$) and 64% ($KV1_{k-1,k}$). The RMSE of Prodan's estimator was increased by 70% in the random patterns. In STIPSI 21, the RMSE of the RDE was increased by 47% when applying $k = 4$ instead of $k = 6$. The increase in RMSE for the KV estimators in STIPSI 21 was between 33% ($KV2_{k-1,k}$) and 47% ($KV1_{k,k+1}$) and was 55% for Prodan's estimator. In the longleaf pine data, the RMSE of RDE was 14% larger for $k = 4$ compared with $k = 6$. The RMSE of the KV estimators was increased by at least 17% ($KV2_{k-1,k}$) and by maximal 28% ($KV1_{k,k+1}$). The RMSE of Prodan's estimator was 30% larger for $k = 4$ than for $k = 6$.

In summary, for all types of tree patterns, such as randomness, regularity (STIPSI 21), and clustering (longleaf pine stand), the biases and the RMSEs of all examined estimators were increased for $k = 4$ compared with $k = 6$. Although the RDE proved to be superior in terms of bias and RMSE for the randomly distributed and clustered tree patterns, the KV2 estimators showed slightly smaller RMSEs for $k = 4$ in the regular tree pattern of STIPSI 21.

Table 4. Simulation results with $k = 4$ of the RDE, KV1 ($KV1_{4,5}$), KV2 ($KV2_{4,5}$), and Prodan's estimator and for $k = 3$ of KV1 ($KV1_{3,4}$) and KV2 ($KV2_{3,4}$).

		RDE			$KV1_{4,5}$			$KV2_{4,5}$			Prodan			$KV1_{3,4}$			$KV2_{3,4}$		
	Trees/ha	Mean	Bias (%)	RMSE	Mean	Bias (%)	RMSE	Mean	Bias (%)	RMSE	Mean	Bias (%)	RMSE	Mean	Bias (%)	RMSE	Mean	Bias (%)	RMSE
Poisson 9	250.0	257.3	2.9	59.2	281.1	12.4	62.7	278.7	11.5	60.7	294.7	17.9	82.6	293.2	17.3	85.4	288.2	15.3	81.0
STIPSI 21	241.9	249.3	3.1	26.8	258.8	7.0	26.0	257.0	6.2	24.6	262.4	8.5	32.3	258.7	7.0	27.7	255.4	5.6	25.4
LP	116.0	115.8	–0.2	31.1	143.0	23.2	54.9	141.7	22.2	54.0	141.5	22.0	50.1	146.2	26.0	55.8	143.8	23.9	53.6

Note: Poisson 9, nine-sample plots in 1000 point patterns generated by a binomial process with a density of 250 trees/ha; STIPSI 21: 250 randomly placed sampling grids of 50 m × 50 m mesh width in STIPSI 21; LP, 250 randomly placed sampling grids of 50 m × 50 m mesh width in the stem map of the longleaf pine data set.

Discussion and conclusions

The proposed RDE approach requires that the positions of all k trees of each sample plot are recorded during the field measurements. The original estimator of Prodan (1968) requires only one distance measurement from the sample point to the kth tree and the estimators of Kleinn and Vilčko (2006*b*) involve additional knowledge about the distance to the $(k + 1)$th tree. As the application of RDE requires additional measurement of the tree coordinates, the utilization of traditional measuring instruments, such as tapes and goniometers, would lead to an increase in survey costs. To minimize these additional costs, a laser distance measuring device should be attached to the existing electronic caliper and a software interface should be available for transferring the data.

The RDE estimator exploits new information from k-tree sample plots that has not been used so far on the intertree and location-to-tree distances. The nearest-neighbor summary characteristics derived from the relatively small sample plot areas appear to give sufficient information to reconstruct tree patterns. Obviously, it does not matter that the estimators $\widehat{D}_l^k(r)$ and $\widehat{H}_{s,m}^k(r)$ obtained from k-tree samples are biased for $D_l(r)$ and $H_{s,m}(r)$.

The reader should note that the SA algorithm used in the present paper is not related to Gibbs process simulation as carried out in other applications of point process statistics (see Illian et al. 2008). In Gibbs process simulation using the Metropolis–Hastings algorithm (Metropolis et al. 1953) or the "birth-and-death" algorithm (Ripley 1987), a stationary Markov chain is simulated, the states of which are point patterns. They aim at simulating an equilibrium state. In contrast, in this paper, an optimal point pattern is determined that minimizes the contrast measure given by eq. 3.

Experience has shown that the most relevant changes in density of the simulated tree pattern occur in the initial phase of the SA (see Fig. 9 for an example). Thus, one can assume to be on the safe side with the conservative choice of $10Q$ iterations, with Q being the initial number of trees affected by possible deletions. A further in-depth analysis should aim at finding an optimum for the required number of iterations, as this would reduce the computational costs.

The allocation of the 10 measurement locations for the estimation of $H_{s,m}^k(r)$ on each sample plot, as shown in Fig. 5, is a successful choice. The use of less than 10 measurement locations was also tested but proved to be inappropriate: the estimated ECDFs became rather discontinuous and showed implausible jumps because of the small amount of distance measurements included.

The application of the RDE method (the algorithm was implemented in R and is available from the corresponding authors upon request) is straightforward regardless of the choice of k. The method proved to be successful for the commonly applied choice of $k = 6$. The RDE works also for $k = 4$ but with a larger bias and RMSE. Obviously, for $k = 4$ in regular tree patterns, the sample plots become too small and the information on intertree and location-to-tree distances is not sufficient for accurate reconstructions. The competing estimators suffer likewise under the reduction to $k = 4$ neighbors. Therefore, it is recommended to use the RDE for density estimation by means of k-tree sampling with $k = 6$.

In this study, the RDE was applied with regard to its potential application in forest inventories. Therefore, the sampling simulations are based on systematic sampling grids instead of a fixed number of sample plots.

The tree density is of course not the only variable of interest in forest inventories. In traditional forest inventories based on simple random sampling, a mean of ratios estimator is usually applied for estimates of most forest stand variables. The global density estimate is then provided by the mean of ratios, each of which is a local density estimate calculated by a fraction with the number of trees on the sample plot in the numerator and the specific plot area in the denominator. To yield global estimates of mean basal area (or volume) per hectare, a mean of products of the local density estimates and the mean basal areas (volume) per tree is calculated. Using biased density estimates in *k*-tree sampling, e.g., through Prodan's estimator, it can be safely assumed that the bias in the density estimate will propagate to biased estimates for the basal area (volume) per hectare.

The RDE density estimate is obtained by dividing the final number of trees in the reduced simulation window by its area. Estimates for the mean basal area per hectare and volume per hectare are then obtained, as previously described, by multiplying the RDE density estimate (trees per hectare) by estimates for mean basal area per tree (square metres per tree) or mean volume per tree (cubic metres per tree) obtained from the original *k*-tree sampling plots.

Assuming that unbiased estimates per tree can be derived from original *k*-tree sample plots, one would also yield unbiased estimates for the mean basal area per hectare and the mean volume per hectare in conjunction with the RDE density estimates.

Acknowledgments

The authors thank Walter Schöpfer and Joachim Hradetzky for providing the STIPSI data and for lively discussions. Arne Pommerening, Juha Lappi, and Alicia Woynowski made useful comments regarding the manuscript. The very constructive and detailed comments of the two anonymous reviewers helped much to improve the quality of the manuscript.

References

Baddeley, A., and Gill, R.D. 1997. Kaplan–Meier estimators of distance distributions for spatial point processes. Ann. Stat. **25**(1): 263–292. doi:10.1214/aos/1034276629.

Cressie, N.A.C. 1991. Statistics for spatial data. John Wiley & Sons, New York.

Diggle, P.J. 1979. On parameter estimation and goodness-of-fit testing for spatial point patterns. Biometrics, **35**(1): 87–101. doi:10.2307/2529938.

Hall, J.B. 1991. Multiple-nearest-tree sampling in an ecological survey of afromontane catchment forest. For. Ecol. Manag. **42**(3–4): 245–266. doi:10.1016/0378-1127(91)90028-T.

Illian, J., Penttinen, A., Stoyan, H., and Stoyan, D. 2008. Statistical analysis and modelling of spatial point patterns. John Wiley & Sons, Chichester UK.

Jonsson, B., Holm, S., and Kallur, H. 1992. A forestry inventory method based on density-adapted circular plot size. Scand. J. For. Res. **7**: 405–421. doi:10.1080/02827589209382733.

Kirkpatrick, S., Gelatt, C.D., Jr., and Vecchi, M.P. 1983. Optimization by simulated annealing. Science, **220**(4598): 671–680. doi:10.1126/science.220.4598.671. PMID:17813860.

Kleinn, C., and Vilčko, F. 2006*a*. Design-unbiased estimation for point-to-tree distance sampling. Can. J. For. Res. **36**(6): 1407–1414. doi:10.1139/X06-038.

Kleinn, C., and Vilčko, F. 2006*b*. A new empirical approach for estimation in *k*-tree sampling. For. Ecol. Manag. **237**(1–3): 522–533. doi:10.1016/j.foreco.2006.09.072.

Krebs, C.J. 1998. Ecological methodology. Addison-Wesley, Reading, Mass.

Lessard, V., Reed, D.D., and Monkevich, N. 1994. Comparing *n*-tree distance sampling with point and plot sampling in northern Michigan forest types. North. J. Appl. For. **11**(1): 12–16.

Lynch, T.B., and Rusydi, R. 1999. Distance sampling for forest inventory in Indonesian teak plantations. For. Ecol. Manag. **113**(2–3): 215–221. doi:10.1016/S0378-1127(98)00427-7.

Magnussen, S., Kleinn, C., and Picard, N. 2008. Two new density estimators for distance sampling. Eur. J. For. Res. **127**(3): 213–224.

Metropolis, N., Rosenbluth, A.W., Rosenbluth, M.N., Teller, A.H., and Teller, E. 1953. Equation of state calculations by fast computing machines. J. Chem. Phys. **21**(6): 1087–1092. doi:10.1063/1.1699114.

Platt, W.J., Evans, G.W., and Rathbun, S.L. 1988. The population dynamics of a long-lived conifer (*Pinus palustris*). Am. Nat. **131**(4): 491–525. doi:10.1086/284803.

Pommerening, A., and Stoyan, D. 2008. Reconstructing spatial tree point patterns from nearest neighbour summary statistics measured in small subwindows. Can. J. For. Res. **38**(5): 1110–1122. doi:10.1139/X07-222.

Prodan, M. 1968. Punktstichprobe für die Forsteinrichtung [Point-to-object distance sampling for forest management planning]. Forst Holzwirt, **23**: 225–226. [In German.]

Ripley, B.D. 1987. Stochastic simulation. John Wiley & Sons, New York.

Schöpfer, W. 1967. Ein Stichprobensimulator für Forschung und Lehre [A sampling simulator for research and teachings]. Allg. Forst Jagdztg. **138**: 267–273. [In German.]

Sloboda, B. 1976. Mathematische und Stochastische Modelle zur Beschreibung der Statik und Dynamik von Bäumen und Beständen — insbesondere das bestandesspezifische Wachstum als stochastischer Prozess [Mathematical and stochastic models for static and dynamic descriptions of trees and forest stands — particularly with regard to growth in forest stands as stochastic processes]. Habilitation thesis, University of Freiburg. [In German.]

Staupendahl, K. 2008. Die modifizierte 6-Baum-Stichprobe — ein geeignetes verfahren zur erfassung von waldbeständen [The modified 6-tree sampling — an appropriate approach for surveys of forest stands]. Allg. Forst Jagdztg. **179**(2/3): 21–33. [In German.]

Tscheschel, A., and Stoyan, D. 2006. Statistical reconstruction of random point patterns. Comput. Stat. Data Anal. **51**(2): 859–871. doi:10.1016/j.csda.2005.09.007.